Chemical vapor deposition and characterization of two-dimensional molybdenum dioxide (MoO_2) nanoplatelets

Nataliia S Vorobeva[1], Alexey Lipatov[1], Dmitry S Muratov[1,2] and Alexander Sinitskii [1,3]
1 Department of Chemistry, University of Nebraska—Lincoln, Lincoln, NE 68588, United States of America
2 National University of Science and Technology 'MISIS', Moscow 119991, Russia
3 Nebraska Center for Materials and Nanoscience, University of Nebraska—Lincoln, Lincoln, NE 68588, United States of America

E-mail: sinitskii@unl.edu

Abstract

We report on the chemical vapor deposition synthesis of MoO_2 nanoplatelets by sublimation of MoO_3 and its reduction in a hydrogen atmosphere at 750 °C. When grown on Si/SiO_2 substrates, the platelets primarily assume a rhomboidal shape and have thicknesses ranging from several to tens of nm. The morphology of MoO_2 crystals was found to depend on the chemical nature of substrates. MoO_2 platelets on Si/SiO_2 were characterized by a number of microscopic and spectroscopic techniques, and the electrical measurements revealed the metallic nature of their conductivity averaging at 2400 ± 1000 S cm^{-1}. Raman spectroscopy of MoO_2 platelets on graphene indicates their strong hole injection property. Small thickness, planar morphology, high chemical stability and metallic conductivity of ultrathin MoO_2 platelets make them potentially interesting for integration different other two-dimensional materials in a variety of electronic structures and devices.

1. Introduction

Ultrathin and two-dimensional (2D) materials have an enormous potential for device applications because they offer very diverse electronic properties and are generally compatible with planar fabrication technologies [1–3]. One of the most studied 2D semiconductors is molybdenum disulfide (MoS_2) [1–5], which showed a great promise for high on-off ratio field-effect transistors (FETs) [6, 7], logic and memory devices [8–10]. Because of its potential for large-scale electronic applications, there was a considerable effort on developing scalable chemical vapor deposition (CVD) procedures to grow large-area films of MoS_2 with controllable thickness [11]. A number of studies utilized a CVD approach that was based on a direct reaction between sulfur vapor and molybdenum trioxide (MoO_3) [11–15]. It was demonstrated that this process happens through an intermediate step that involves partial reduction of MoO_3 to molybdenum dioxide (MoO_2) [16] in a form of thin rhomboidal platelets [17, 18], which then react with sulfur to produce MoS_2. These MoO_2 platelets were reported in several publications on CVD growth of MoS_2 but have rarely been a focus of separate studies [19, 20]. Small thickness and planar morphology of these platelets, as well as the known high metallic conductivity and chemical stability of MoO_2, make ultrathin

MoO_2 crystals potentially interesting for integration with different 2D materials in a variety of electronic structures and devices [5].

MoO_2 has a monoclinic structure (figure 1(a)) with the space group $P2_1/c$, lattice constants of a = 5.6109 Å, b = 4.8562 Å, and c = 5.6285 Å, and the monoclinic angle β = 120.95° [21]. This is a distorted rutile structure that consists of MoO_6 octahedra connected through the oxygen atoms in the corners, but the unit cell contains four MoO_2 formula units as opposed to two in rutile [22]. Figure 1(a) shows that MoO_2 is not a van der Waals crystal like bulk graphite, h-BN or MoS_2, for which exfoliation or direct growth of monolayer and few-layered sheets is expected from the crystal structure perspective. However, this study shows that MoO_2 has a tendency to form few-nm thin platelets with uniform surfaces, which could be comparable in thickness and appearance to few-layered stacks of conventional 2D materials.

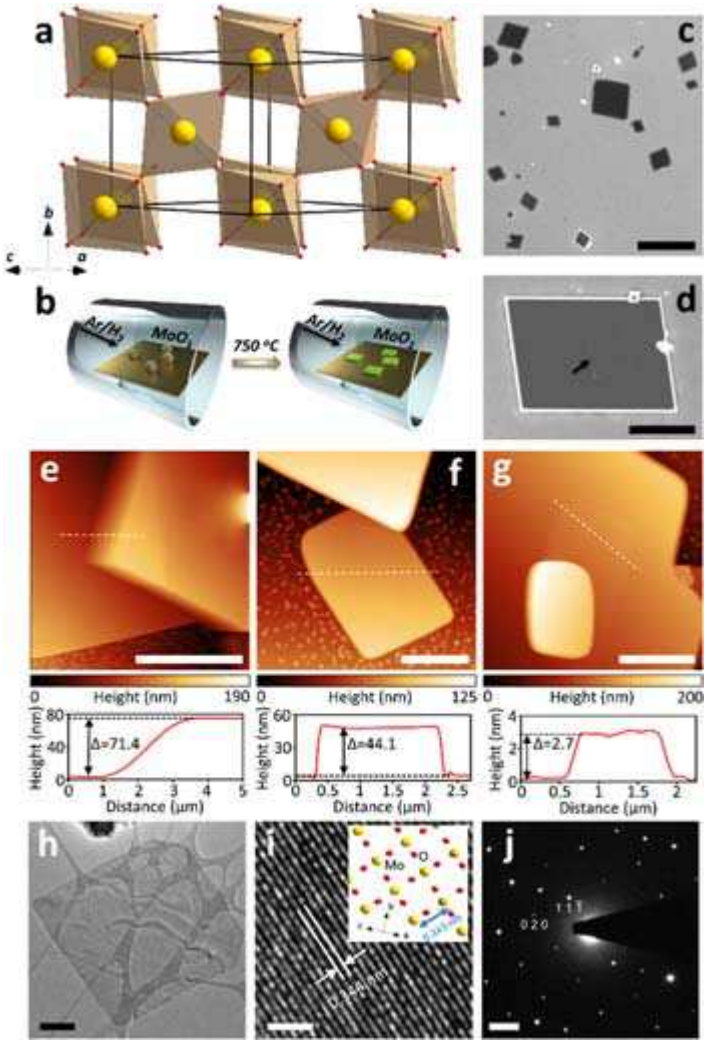

Figure 1. Chemical vapor deposition and microscopic characterization of MoO_2 platelets. (a) Unit cell of MoO_2. Yellow spheres—Mo, red spheres—O. (b) Scheme of CVD growth of MoO_2platelets; see text for details. (c) SEM image of MoO_2 platelets on a Si/SiO_2 substrate. Scale bar is 5 μm. (d) SEM image of thin MoO_2 crystal (shown by the black arrow) on the surface of a larger platelet. Scale bar is 2 μm. (e)–(g) AFM images of MoO_2 platelets along with corresponding height profiles. Scale bars are (e) 5 μm and (f), (g) 2 μm. (h) TEM image of a MoO_2 platelet on a TEM grid. Scale bar is 0.5 μm. (i) High-resolution TEM

image of the MoO_2platelet shown in panel (h). Scale bar is 2 nm. (j) Selected area electron diffraction pattern of the MoO_2 crystal shown in (h), (i). Scale bar is 2 nm^{-1}.

Because of its high conductivity and chemical stability, molybdenum dioxide has been studied for a number of applications mostly related to energy storage [23–29] and catalysis [30, 31]. These applications primarily required bulk forms of MoO_2 that can be synthesized by a wide range of techniques including thermal decomposition of various molybdates [23, 28, 31], hydrothermal method [25, 26] and reduction of MoO_3 with hydrogen [29, 32, 33] or ethanol vapor [27]. The MoO2materials prepared by these methods greatly varied in their morphologies, which included nanoparticles [26, 27], nanorods [23, 32, 33], nanosheets [25], hollow [24] and mesoporous particles [28], and interwoven structures [29] among others.While bulk synthetic approaches enable MoO_2 materials with very diverse morphologies, the formation of MoO_2 platelets during the synthesis of MoS_2 provides new opportunities. In particular, as these thin flat crystals form on Si/SiO_2 substrates [17], they could be directly used for the device fabrication and electrical measurements. However, while sulfur is used to produce MoS_2 from MoO_3, if MoO_2 platelets are considered as the target product of the synthesis, then it does not appear to be a necessary reagent. Therefore, in this study we investigated the direct conversion of MoO_3 to MoO_2 in a hydrogen atmosphere at high temperature with the goal of producing thin MoO_2 platelets and measuring their electronic properties.

There were several recent reports on the electrical characterization of individual MoO_2 crystals, and their conductivities varied considerably [19, 20, 33]. The platelets grown via the reaction of $MoO_3$and sulfur were shown to have electrical conductivity of 3600 S cm^{-1} [19], while those produced by the hydrogen reduction of MoO_3 exhibited considerably lower conductivities of 200–475 S cm^{-1} [20]. MoO_2 nanorods prepared by the hydrogen reduction of MoO_3 nanobelts were shown to have electrical conductivities ranging from 80 to 400 S cm^{-1} [33].

In this paper, we present a CVD procedure for the synthesis of metallic MoO_2 platelets with conductivities of about 2400 ± 1000 S cm^{-1} by the direct reduction of MoO_3 in a hydrogen atmosphere at 750 °C without a sulfur reagent. The platelets were primarily grown on Si/SiO_2substrates, on which they were characterized by a number of methods, including scanning electron microscopy (SEM), scanning atomic force microscopy (AFM), transmission electron microscopy (TEM), Raman spectroscopy and x-ray photoelectron spectroscopy (XPS). However, the morphology of MoO_2 crystals was found to depend on the chemical nature of substrates, which highlights the possibility of their controlled growth to suit specific applications.

2. Results and discussion

Figure 1(b) shows the scheme of the CVD growth of MoO_2 platelets. In a typical synthesis, 0.5–10 mg of MoO_3 powder (Sigma-Aldrich, ≥99.5%) was placed on a substrate of interest, which was placed in a tube furnace (Lindberg Blue M). While the majority of experiments were performed using p-type Si substrates covered with 300 nm thick SiO_2, we also studied MoO_2 growth on other substrates, such as quartz crystals, Cu and Ni foils, and graphene. The tube was evacuated to the pressure of 130 mTorr, and under the stream of 50 sccm of Ar and 10 sccm of H_2 the substrate was heated up to 750 °C at a rate of 10 °C min^{-1} and annealed for 1 h. Then the furnace was turned off and the substrate was cooled down to room temperature. During the annealing, randomly shaped particles of MoO_3convert to rhomboidal MoO_2 platelets. A representative SEM image of such platelets on a Si/SiO_2substrate is shown in figure 1(c). SEM was performed using a Zeiss Supra 40 field-emission scanning electron microscope at the accelerating voltage of 5 kV. While the majority of the MoO_2 platelets appear to have flat surfaces, in some cases we observed the

formation of terraces as shown in figure 1(d). Interestingly, the appearance of such structures is reminiscent of layered compounds, even though MoO_2 is not a van der Waals crystal (figure 1(a)). In order to examine the morphology of MoO_2 crystals we employed AFM, which was performed using a Digital Instruments Nanoscope IIIa Dimension 3100 system. Figures 1(e)–(g) show several scenarios of assemblies of MoO_2 platelets grown on Si/SiO_2. While most platelets form parallel to the substrate, some grow over adjacent MoO_2 crystals and are thus tilted relative to the Si/SiO_2 surface (figure 1(e)). A typical MoO_2 platelet that is parallel to the substrate is shown in figure 1(f). The height profile measured along the dashed line shows that this particular platelet is 44 nm thick. Other MoO_2 crystals that were measured in this and similar samples varied in thickness from ~3 to over 100 nm. Figure 1(g) shows two MoO_2 crystals that formed on a surface of a larger crystal. The smallest crystal is ~2.7 nm thick, which indicates that the MoO_2 feature sizes could be comparable with thicknesses of few-layered stacks of conventional 2D materials. The curved edges and rounded corners of the MoO_2 platelets suggest that the energy difference between different in-plane crystalline directions is likely smaller than for various transition metal dichalcogenides, such as MoS_2, which are known to form well-defined triangles with straight edges and sharp corners upon CVD growth [11–15].

MoO_2 platelets were also studied by TEM. MoO_2 crystals were transferred from Si/SiO_2 substrates on TEM grids as described elsewhere [34], using polymethyl methacrylate (PMMA) as a support for the transfer and a 5% HF solution to etch SiO_2. TEM was performed using a FEI Tecnai Osiris transmission electron microscope operated at the accelerating voltage of 200 kV. Figure 1(h) shows TEM image of a thin MoO_2 crystal on a TEM grid. A high-resolution TEM image (figure 1(i)) demonstrates the lattice spacing of 0.344 nm, which perfectly matches the $(11\bar{1})$ interplanar distance in the MoO_2 crystal structure; the inset in figure 1(i) shows the corresponding crystal orientation. The latter is further supported by a selected area electron diffraction (SAED) pattern (figure 1(j)), which shows a well-defined set of diffraction spots confirming high crystallinity of the MoO_2 platelets. SAED diffraction pattern was post-processed using Crystallographic Tool Box (CrysTBox) software [35].

The surface composition of the sample was characterized by XPS, which was performed using a Thermo Scientific K-Alpha x-ray photoelectron spectrometer. For the XPS analysis, the crystals were grown on Cu foils instead of Si/SiO_2 to minimize the surface charging and the contribution of the substrate oxygen to the O1*s* spectra of MoO_2. The integration of the Mo3*d* and O1*s* core level spectra of the as-grown samples yielded the chemical composition of $MoO_{2.15}$, which indicates the surface contamination and the formation of MoO_3 due to the sample storage in ambient conditions. Although the surface of MoO_2 platelets oxidizes in air, the thin MoO_3 layer likely passivates the bulk of the crystals, as the platelets that were exposed to ambient conditions for several months retained their characteristic rhomboidal shape and produced similar spectroscopic (XPS, Raman) data to as-grown samples. The surface contamination was evidenced by the presence of fitting components in the O1*s* spectrum at 531.9 and 533.3 eV, which are characteristic for oxygen in organic compounds, as well as the XPS signal in the C1*s* region around 284.5 eV. The surface cleaning of the samples by the argon ion bombardment for 1 min removed these O1*s* fitting components, as well as the C1*s*peak, and the resulting XPS Mo3*d* and O1*s* spectra are shown in figures 2(a), (b). The Mo3*d* peak consists of three components. Screened final state peaks for MoO_2 are located at ~229.2 ($Mo3d_{5/2}$) and ~232.48 eV ($Mo3d_{3/2}$). Unscreened final state peaks for MoO_2 are located at ~230.81 ($Mo3d_{5/2}$) and ~234.28 eV ($Mo3d_{3/2}$). The energy difference between the screened and unscreened $Mo3d_{5/2}$peaks is 1.61 eV, which is close to the plasmon energy of 1.56 eV for MoO_2 measured by electron energy loss spectroscopy [36]. Other peaks located at ~228.3 and ~230.88 eV correspond to the metallic molybdenum, which formed due to

the reduction of MoO_2 by the argon sputtering; these peaks were not included in the peak integration for assessing the Mo:O atomic ratio. Figure 2(b) shows the fitted O1*s* core level peak containing two states. The main O1*s* peak is located at ~530.49 eV, and the shoulder at ~531.51 eV is a satellite. The shapes and positions of the Mo3*d* and O1*s* peaks are in good agreement with the prior literature report [21]. The integration of the Mo3*d* and O1*s*spectra of the sample after the Ar cleaning produced the chemical composition of $MoO_{1.96}$, which is in perfect agreement with the expected Mo:O atomic ratio of 1:2.

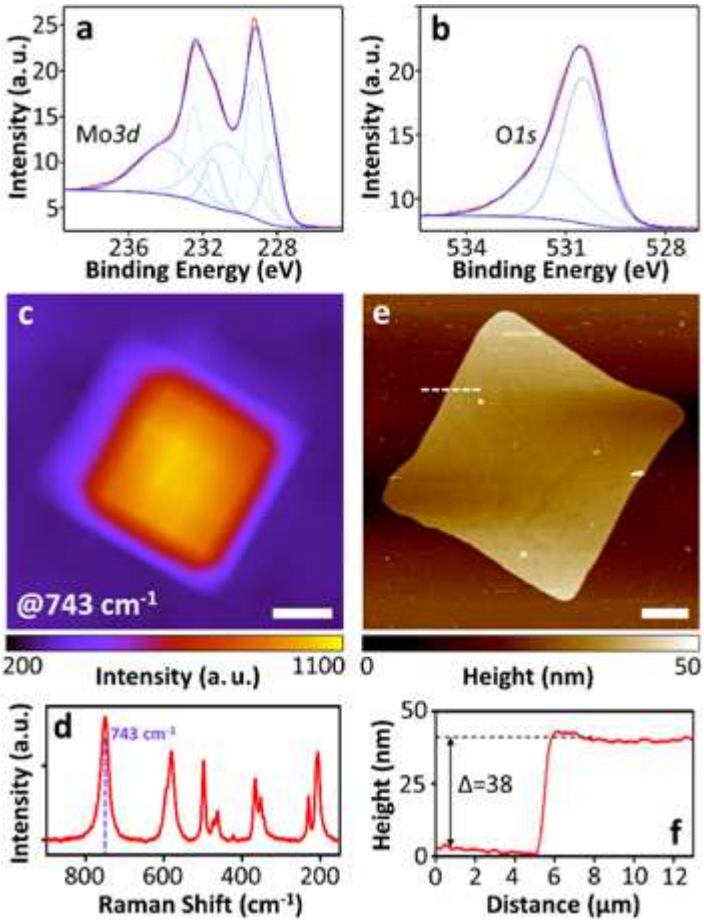

Figure 2. Spectroscopic characterization of MoO_2 platelets. (a) XPS Mo3*d* core level spectrum of MoO_2 grown on a Cu foil. (b) XPS O1*s* core level spectrum of MoO_2 grown on a Cu foil. In (a) and (b) the red curves represent experimental spectra and the blue curves show their fittings. (c) Raman intensity map of a MoO_2 platelet on Si/SiO_2 recorded at 743 cm^{-1}. Scale bar is 2 μm. (d) Raman spectrum of CVD-grown MoO_2. The 743 cm^{-1} peak is shown by the purple dashed line. (e) AFM image of the same MoO_2 platelet as in (c). Scale bar is 1 μm. (f) AFM height profile of the MoO_2 platelet measured along the white dashed line in panel (e).

MoO_2 can also be distinguished from MoO_3 by Raman spectroscopy [37–39]. Raman spectroscopy was performed using a Thermo Scientific DXR Raman microscope with a 532 nm excitation laser. Figure 2(c) shows a Raman map of a CVD-grown MoO_2 platelet on Si/SiO_2 that was recorded at 743 cm^{-1}, which corresponds to the position of the most intense line in the Raman spectrum of MoO_2(figure 2(d)); the map shows uniform signal from the platelet. Other intense lines in the spectrum include 127, 207, 230, 350, 365, 499, 556 and 572 cm^{-1}, which agree well

with prior literature reports [19, 39]. The Raman map and the spectrum were recorded from the MoO_2 platelet that is demonstrated in figure 2(e). According to the AFM height profile that is shown in figure 2(f), this platelet was 38 nm thick.

The described CVD procedure can be used to grow MoO_2 crystals not only on Si/SiO_2 but also on a variety of other thermally stable substrates. For example, we found that rhomboidal platelets similar to the ones shown in figure 1(c) can be grown on quartz single crystals. MoO_2 crystals were also observed on metal substrates, such as Cu and Ni foils. Figure 3(a) shows a representative SEM image of MoO_2 crystals on Cu. Interestingly, these samples look less uniform than MoO_2 platelets on Si/SiO_2 (figure 1(c)) in terms of their shape and orientation relative to the substrate. In particular, the crystals do not predominantly lay flat but form at random tilt angles relative to the substrate. This morphology is further illustrated by figure 3(b), which shows a tilted view SEM image of MoO_2platelets on Cu. Qualitatively similar morphology was also found for MoO_2 platelets grown on a Ni foil.

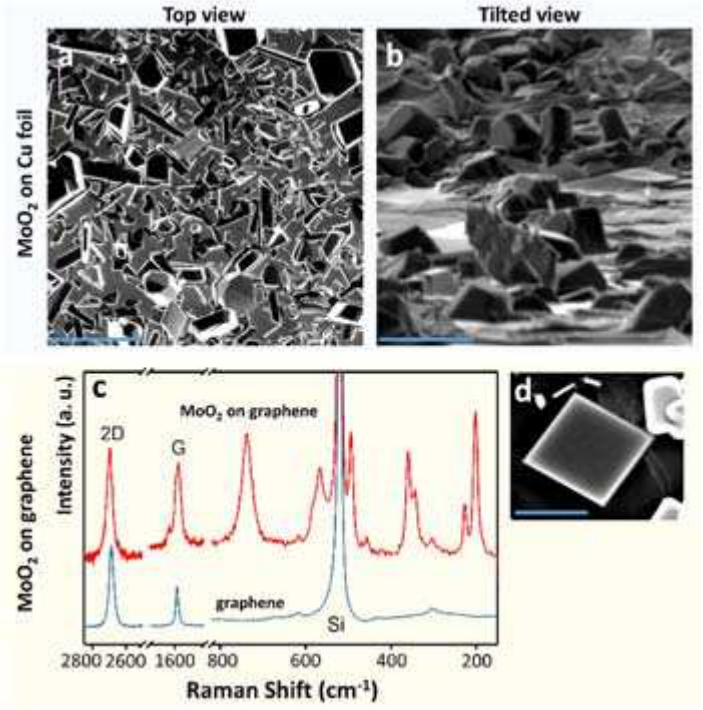

Figure 3. CVD growth of MoO_2 crystals on different substrates. (a), (b) SEM images of MoO_2crystals grown on a Cu foil: (a) top view and (b) tilted view. Scale bars are 5 μm. (c) Raman spectra of the CVD-grown graphene (bottom) and MoO_2 platelets grown on graphene (top). (d) SEM image of MoO_2 platelet on graphene. Scale bar is 1 μm.

One parameter that could be used to compare these substrates is their roughness. Using AFM, we found comparably small root mean squared (rms) values for Si/SiO_2 (~0.3 nm) and quartz (~0.4 nm) substrates, on which the CVD-grown MoO_2 crystals predominantly laid flat. Rolled Cu foils had a visible texture of periodic grooves producing much larger rms roughness values of about 50 nm that varied considerably for different sample areas. Therefore, random orientation of MoO_2 crystals on Cu substrates could in part be related to their large roughness. However, MoO_2 crystals also grew at different tilt angles relative to substrate on smoother Ni foils (rms roughness ~3 nm), suggesting that the substrate's roughness may not be the only parameter

responsible for the planar or tilted growth of MoO_2 platelets. Overall, these results demonstrate that substrate can affect the growth mode of MoO_2crystals.

In addition to testing bulk substrates, such as quartz and metal foils, we also attempted to grow MoO_2crystals on graphene. Such growth can result in graphene/MoO_2 heterostructures, which could be interesting from the point of view of materials integration for electronic applications. For this experiment, monolayer graphene was grown by CVD on a copper foil at 1000 °C using methane as the carbon source and then transferred to a Si/SiO_2 substrate [40]; details of the growth and transfer procedures can be found in our previous work [34]. Figure 3(c) shows the Raman spectrum of the as-prepared graphene on Si/SiO_2 with characteristic spectroscopic signatures of monolayer graphene, which include G and 2D bands at 1590 and 2685 cm^{-1}, respectively, and a G-to-2D intensity ratio of 2 [41]. After the MoO_2 growth, the Raman spectrum of the sample exhibits a superposition of peaks corresponding to monolayer graphene and MoO_2 (figure 3(c)). Interestingly, after the growth of MoO_2 the G and 2D bands shift to 1585 and 2696 cm^{-1}, respectively, indicating strong hole doping of graphene [42, 43]. This observation is in line with the previous reports on the hole injection by MoO_2in organic hole-transporting layers [44] and MoS_2 FETs with MoO_x ($x < 3$) electrodes [45]. SEM image in figure 3(d) shows a rhomboidal MoO_2 crystal on a Si/SiO_2/graphene substrate (rms roughness ~0.7 nm), which is similar in appearance to MoO_2 platelets grown directly on Si/SiO_2(figure 1).

Finally, we assessed the electronic properties of the MoO_2 platelets grown on Si/SiO_2 substrates. Two-terminal devices, in which MoO_2 crystals bridged Cr/Au (3 nm/12 nm) electrodes were fabricated by standard electron-beam lithography followed by electron-beam evaporation; the detailed procedure that we used for the device fabrication can be found in [46]. The top inset in figure 4 shows an AFM image of one of the eight devices prepared in this work. This particular device is based on a MoO_2platelet that is 7.5 nm thick. In other devices the thicknesses of MoO_2 platelets varied from 5.4 to 24 nm. For the platelets in this thickness range we did not observe a correlation between the crystals' thicknesses and their electrical conductivities.

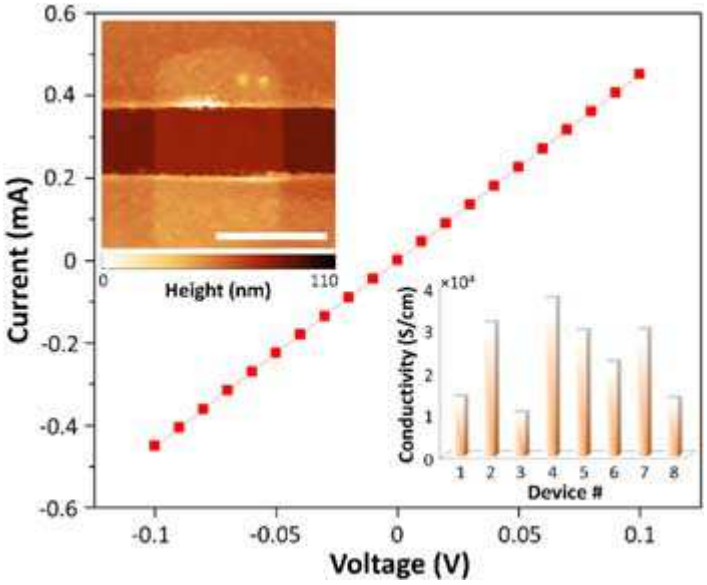

Figure 4. Electrical measurements of MoO_2 platelets. *I–V* dependence for the MoO_2 device shown in the AFM image in the top left inset (scale bar is 1 μm). The bottom right inset shows electrical conductivities of eight MoO_2 devices.

The electrical measurements of MoO_2 devices were performed in a Lake Shore TTPX cryogenic probe station at the base pressure of about 2×10^{-6} Torr; the devices were evacuated for at least 2 days before the measurements to minimize the effect of surface adsorbates [47]. The electrical characteristics of the devices were recorded using an Agilent 4155C semiconductor parameter analyzer. Figure 4 shows a current (I)—voltage (V) dependence for the MoO_2 device shown in the inset. The device exhibits an Ohmic behavior with a conductivity of 2223 S cm^{-1}. Since the devices were prepared on heavily doped p-type Si, which was covered by a 300 nm thick SiO_2, the electrically conductive silicon substrate could be used as a gate electrode to test the effect of an electric field on the conductivity of thin MoO_2 platelets. The in-plane I–V dependencies did not change when the gate voltage was modulated from −40 to 40 V (in figure 4, we therefore do not plot the I–Vdependencies measured at different gate voltages, because the completely overlap), confirming the metallic nature of the conductivity of MoO_2. The bottom inset in figure 4 summarizes the results of the conductivity measurements of eight MoO_2 devices. The conductivities varied from 1040 to 3725 S cm^{-1} with the mean value of 2400 ± 1000 S cm^{-1}. This value is comparable to the results of electrical measurements of MoO_2 platelets grown via the reaction of MoO_3 and sulfur (3600 S cm^{-1}) [19], and about an order of magnitude better than the previously reported conductivities of MoO_2 platelets (200–475 S cm^{-1}) [20] and nanorods (80–400 S cm^{-1}) [33] grown using the hydrogen reduction of MoO_3. Our results demonstrate that highly conductive MoO_2 platelets can be grown by a direct conversion from MoO_3 in a hydrogen atmosphere without the need of sulfur.

In summary, we demonstrated the CVD synthesis of MoO_2 nanoplatelets by sublimation of $MoO_3$and its reduction in a hydrogen atmosphere at 750 °C. When grown on Si/SiO_2 substrates, the platelets primarily assume a rhomboidal shape and have thicknesses ranging from several to tens of nm. The morphology of MoO_2 crystals was found to depend on the chemical nature of a substrate. MoO_2 platelets on Si/SiO_2 were characterized by several microscopic and spectroscopic techniques, and the electrical measurements revealed that the crystals have a metallic conductivity averaging at 2400 ± 1000 S cm^{-1}. Furthermore, Raman spectroscopy of MoO_2 platelets on graphene indicates their hole injection ability. Small thickness, planar morphology, high chemical stability and metallic conductivity of ultrathin MoO_2 platelets make them potentially interesting for integration with different 2D materials in a variety of electronic structures and devices.

Acknowledgments

This work was supported by the National Science Foundation (NSF) through the Nebraska Materials Research Science and Engineering Center (MRSEC) (grant no. DMR-1420645) and ECCS-1740136, as well as by the NCORE, a wholly owned subsidiary of the Semiconductor Research Corporation (SRC). The materials characterization was performed in part in MISIS, in which the work was supported by the Ministry of Education and Science of the Russian Federation (K2-2016-033), and in the Nebraska Nanoscale Facility, which is supported by the NSF (ECCS-1542182) and the Nebraska Research Initiative.

References

[1] Fiori G, Bonaccorso F, Iannaccone G, Palacios T, Neumaier D, Seabaugh A, Banerjee S K and Colombo L 2014 Electronics based on two-dimensional materials Nat. Nanotechnol. **9** 768

[2] Wang Q H, Kalantar-Zadeh K, Kis A, Coleman J N and Strano M S 2012 Electronics and optoelectronics of two-dimensional transition metal dichalcogenides Nat. Nanotechnol. **7** 699
[3] Jariwala D, Sangwan V K, Lauhon L J, Marks T J and Hersam M C 2014 Emerging device applications for semiconducting two-dimensional transition metal dichalcogenides ACS Nano **8** 1102
[4] Butler S Z et al 2013 Progress, challenges, and opportunities in two-dimensional materials beyond graphene ACS Nano **7** 2898
[5] Geim A K and Grigorieva I V 2013 Van der Waals heterostructures Nature **499** 419
[6] Radisavljevic B, Radenovic A, Brivio J, Giacometti V and Kis A 2011 Single-layer MoS2 transistors Nat. Nanotechnol. **6** 147
[7] Baugher B W H, Churchill H O H, Yang Y and Jarillo-Herrero P 2013 Intrinsic electronic transport properties of high-quality monolayer and bilayer MoS2 Nano Lett. **13** 4212
[8] Wang H, Yu L, Lee Y-H, Shi Y, Hsu A, Chin M L, Li L-J, Dubey M, Kong J and Palacios T 2012 Integrated circuits based on bilayer MoS2 transistors Nano Lett. **12** 4674
[9] Lipatov A, Sharma P, Gruverman A and Sinitskii A 2015 Optoelectrical molybdenum disulfide (MoS2)—ferroelectric memories ACS Nano **9** 8089
[10] Li T et al 2017 Polarization-mediated modulation of electronic and transport properties of hybrid MoS2–BaTiO3–SrRuO3 tunnel junctions Nano Lett. **17** 922
[11] Shi Y, Li H and Li L-J 2015 Recent advances in controlled synthesis of two-dimensional transition metal dichalcogenides via vapour deposition techniques Chem. Soc. Rev. **44** 2744
[12] Lee Y-H et al 2012 Synthesis of large-area MoS2 atomic layers with chemical vapor deposition Adv. Mater. **24** 2320
[13] Najmaei S, Liu Z, Zhou W, Zou X, Shi G, Lei S, Yakobson B I, Idrobo J-C, Ajayan P M and Lou J 2013 Vapour phase growth and grain boundary structure of molybdenum disulphide atomic layers Nat. Mater. **12** 754
[14] Lee Y-H et al 2013 Synthesis and transfer of single-layer transition metal disulfides on diverse surfaces Nano Lett. **13** 1852
[15] van der Zande A M, Huang P Y, Chenet D A, Berkelbach T C, You Y, Lee G-H, Heinz T F, Reichman D R, Muller D A and Hone J C 2013 Grains and grain boundaries in highly crystalline monolayer molybdenum disulphide Nat. Mater. **12** 554
[16] Lin Y-C, Zhang W, Huang J-K, Liu K-K, Lee Y-H, Liang C-T, Chu C-W and Li L-J 2012 Wafer-scale MoS2 thin layers prepared by MoO3 sulfurization Nanoscale **4** 6637
[17] Wang X, Feng H, Wu Y and Jiao L 2013 Controlled synthesis of highly crystalline MoS2 flakes by chemical vapor deposition J. Am. Chem. Soc. **135** 5304
[18] Li X L and Li Y D 2003 Formation of MoS2 inorganic fullerenes (IFs) by the reaction of MoO3 nanobelts and S Chemistry—A Eur. J. **9** 2726
[19] Li J, Yin J, Li X, Zhou J and Guo W 2016 Chemical vapor deposition of ultra-thin molybdenum dioxide nanosheets Mater. Lett. **174** 188
[20] Pu E, Liu D, Ren P, Zhou W, Tang D, Xiang B, Wang Y and Miao J 2017 Ultrathin MoO2 nanosheets with good thermal stability and high conductivity AIP Adv. **7** 025015
[21] Scanlon D O, Watson G W, Payne D J, Atkinson G R, Egdell R G and Law D S L 2010 Theoretical and experimental study of the electronic structures of MoO3 and MoO2 J. Phys. Chem. C **114** 4636
[22] Magneli A and Andersson G 1955 On the MoO2 structure type Acta Chem. Scand. A **9** 1378
[23] Rajeswari J, Kishore P S, Viswanathan B and Varadarajan T K 2009 One-dimensional MoO2 nanorods for supercapacitor applications Electrochem. Commun. **11** 572

[24] Liu J, Tang S, Lu Y, Cai G, Liang S, Wang W and Chen X 2013 Synthesis of Mo2N nanolayer coated MoO2 hollow nanostructures as high-performance anode materials for lithium-ion batteries Energy Environ. Sci. **6** 2691
[25] Yang L C, Gao Q S, Zhang Y H, Tang Y and Wu Y P 2008 Tremella-like molybdenum dioxide consisting of nanosheets as an anode material for lithium ion battery Electrochem. Commun. **10** 118
[26] Liang Y, Yang S, Yi Z, Sun J and Zhou Y 2005 Preparation, characterization and lithium-intercalation performance of different morphological molybdenum dioxide Mater. Chem. Phys. **93** 395
[27] Yang L C, Gao Q S, Tang Y, Wu Y P and Holze R 2008 MoO2 synthesized by reduction of MoO3 with ethanol vapor as an anode material with good rate capability for the lithium ion battery J. Power Sources **179** 357
[28] Shi Y, Guo B, Corr S A, Shi Q, Hu Y-S, Heier K R, Chen L, Seshadri R and Stucky G D 2009 Ordered mesoporous metallic MoO2 materials with highly reversible lithium storage capacity Nano Lett. **9**4215
[29] Sun Y, Hu X, Yu J C, Li Q, Luo W, Yuan L, Zhang W and Huang Y 2011 Morphosynthesis of a hierarchical MoO2 nanoarchitecture as a binder-free anode for lithium-ion batteries Energy Environ. Sci. **4** 2870
[30] Solymosi F, Cserényi J, Szöke A, Bánsági T and Oszkó A 1997 Aromatization of methane over supported and unsupported Mo-based catalysts J. Catal. **165** 150
[31] Itika K, Babu G V R, Jayesh T B, Rao K S R and Nagaraja B M 2017 Synchronized dehydrogenation-hydrogenation reactions over partially reduced MoO2 based catalyst for simultaneous synthesis of styrene and aniline Catal. Commun. **90** 27
[32] Satishkumar B C, Govindaraj A, Nath M and Rao C N R 2000 Synthesis of metal oxide nanorods using carbon nanotubes as templates J. Mater. Chem. **10** 2115
[33] Hu B, Mai L, Chen W and Yang F 2009 From MoO3 nanobelts to MoO2 nanorods: structure transformation and electrical transport ACS Nano **3** 478
[34] Lu H, Lipatov A, Ryu S, Kim D J, Lee H, Zhuravlev M Y, Eom C B, Tsymbal E Y, Sinitskii A and Gruverman A 2014 Ferroelectric tunnel junctions with graphene electrodes Nat. Commun. **5** 5518
[35] Klinger M and Jager A 2015 Crystallographic tool box (CrysTBox): automated tools for transmission electron microscopists and crystallographers J. Appl. Crystallogr. **48** 2012
[36] Gulino A, Parker S, Jones F H and Egdell R G 1996 Influence of metal-metal bonds on electron spectra of MoO2 and WO2 J. Chem. Soc. Faraday Trans. **92** 2137
[37] Spevack P A and McIntyre N S 1992 Thermal reduction of molybdenum trioxide J. Phys. Chem. **96**9029
[38] Spevack P A and McIntyre N S A R 1993 and XPS investigation of supported molybdenum oxide thin films: I. Calcination and reduction studies J. Phys. Chem. **97** 11020
[39] Dieterle M and Mestl G 2002 Raman spectroscopy of molybdenum oxides: II. Resonance Raman spectroscopic characterization of the molybdenum oxides Mo4O11 and MoO2 Phys. Chem. Chem. Phys. **4** 822
[40] Li X S et al 2009 Large-area synthesis of high-quality and uniform graphene films on copper foils Science **324** 1312
[41] Ferrari A C et al 2006 Raman spectrum of graphene and graphene layers Phys. Rev. Lett. **97** 187401

[42] Pisana S, Lazzeri M, Casiraghi C, Novoselov K S, Geim A K, Ferrari A C and Mauri F 2007 Breakdown of the adiabatic Born–oppenheimer approximation in graphene Nat. Mater. **6** 198
[43] Das A et al 2008 Monitoring dopants by Raman scattering in an electrochemically top-gated graphene transistor Nat. Nanotechnol. **3** 210
[44] Matsushima T and Adachi C 2008 Enhanced hole injection and transport in molybdenum-dioxide-doped organic hole-transporting layers J. Appl. Phys. **103** 034501
[45] Chuang S et al 2014 MoS2 p-type transistors and diodes enabled by high work function MoOx contacts Nano Lett. **14** 1337
[46] Lipatov A, Wilson P M, Shekhirev M, Teeter J D, Netusil R and Sinitskii A 2015 Few-layered titanium trisulfide (TiS3) field-effect transistors Nanoscale **7** 12291
[47] Sinitskii A, Dimiev A, Kosynkin D V and Tour J M 2010 Graphene nanoribbon devices produced by oxidative unzipping of carbon nanotubes ACS Nano **4** 5405